Benchmark Dyson Orbital Study of the Ionization Spectrum and Electron Momentum Distributions of Ethanol in Conformational Equilibrium

Filippo Morini, Balázs Hajgató,† and Michael S. Deleuze*

Research Group of Theoretical Chemistry, Department SBG, Hasselt University, Agoralaan Gebouw D, B-3590 Diepenbeek, Belgium

Chuan G. Ning and Jing K. Deng

Department of Physics and Key Laboratory of Atomic and Molecular NanoSciences of MOE, Tsinghua University, Beijing 100084, People's Republic of China

Received: May 14, 2008; Revised Manuscript Received: July 10, 2008

An extensive study, throughout the valence region, of the electronic structure, ionization spectrum, and electron momentum distributions of ethanol is presented, on the ground of a model that focuses on a mixture of the *gauche* and *anti* conformers in their energy minimum form, using weight coefficients obtained from thermostatistical calculations that account for the influence of hindered rotations. The analysis is based on accurate calculations of valence one-electron and shakeup ionization energies and of the related Dyson orbitals, using one-particle Green's Function (1p-GF) theory in conjunction with the so-called third-order Algebraic Diagrammatic Construction scheme [ADC(3)]. The confrontation against available UPS (HeI) measurements indicates the presence in the spectral bands of significant conformational fingerprints at outer-valence ionization energies ranging from ∼14 to ∼18 eV. The shakeup onset is located at ∼24 eV, and a shoulder at ∼14.5 eV in the He I spectrum can be specifically ascribed to the minor *anti* (C_s) conformer fraction. Thermally and spherically averaged Dyson orbital momentum distributions are computed for seven resolvable bands in model (e, 2e) ionization spectra at an electron impact energy of 1.2 keV. A comparison is made with results obtained from standard (B3LYP) Kohn−Sham orbitals and EMS measurements employing a high-resolution spectrometer of the third generation. The analysis is qualitatively in line with experiment and reveals a tremendously strong influence of the molecular conformation on the outermost electron momentum distributions. Quantitatively significant discrepancies with experiment can nonetheless be tentatively ascribed to strong dynamical disorder in the gas phase molecular structure.

Introduction

Most molecules exist in more than one conformation, corresponding to different degrees of internal rotation of one molecular fragment relative to another. The determination of the influence of the molecular conformation on the underlying electronic structure and wave function has been over the last two decades a topic of growing interest, both from a fundamental viewpoint and with regard to the structural and chemical characterization of industrially important polymer surfaces and organic thin films. Various ionization techniques have been used to this end, including photoelectron spectroscopy [XPS, ultraviolet photoelectron spectroscopy (UPS), and synchrotron PES],[1] electron momentum spectroscopy (EMS),[2] or Penning electron ionization spectroscopy.[3] Among these techniques, EMS[4] is probably the most attractive, as it combines the principles of scattering and ionization experiments for experimentally reconstructing in momentum space one-electron transition densities that are associated to specific ionization channels and which can be assimilated to orbital momentum densities if a one-electron picture of ionization prevails. In practice, orbital momentum distributions are specifically inferred from an angular analysis of ionization intensities in binary (e, 2e) electron impact ionization experiments ($M + e^- \rightarrow M^+ + 2e^-$) at high kinetic energies and under a nonplanar symmetric kinematical setup. When applied to structurally versatile systems, this powerful spectroscopy enables extensive studies, throughout the valence region, of the influence of the molecular conformation on both the electron binding energies and the corresponding electron densities in momentum space.[2,5] In simpler words, with this technique, one can thus in principle directly "image" the interplay between the molecular conformation and the valence molecular orbitals. In practice, the interpretation of EMS experiments onto structurally flexible molecules requires extensive theoretical work if it has to have any value at all, because these experiments are subject to all of the complications that may arise with ionization processes, such as a breakdown of the orbital picture of ionization and a dispersion of the ionization intensity over excited electronic (shakeup) configurations of the cation,[6] thermally induced molecular motions in the ground state and vibronic coupling interactions,[7] or postcollision and distorted wave effects.[8] One of the main requirements for correctly unraveling the results of such experiments (see ref 2d in particular) is a correct assignment of spectral bands that accounts for the influence of the molecular conformation onto the ionization energies and related spectroscopic strengths.

A recent carbon 1s photoelectron study on ethanol[9] indicates that detailed pieces of information on the molecular conformation are also experimentally amenable from an analysis of the

* To whom correspondence should be addressed. E-mail: michael.deleuze@uhasselt.be.

† Present address: General Chemistry Division, Free University of Brussels, Pleinlaan 2, B-1050 Brussels, Belgium.

10.1021/jp804284p CCC: $40.75
Published on Web 08/30/2008

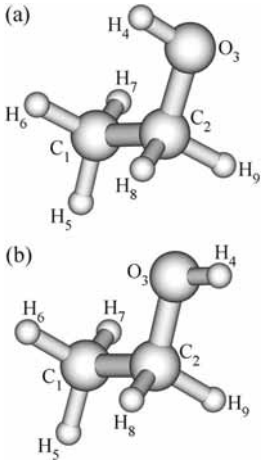

Figure 1. Molecular structures of ethanol calculated at the B3LYP/aug-cc-pVTZ level: (a) C_1 and (b) C_s species.

core ionization bands. Most studies[1−3] of the interplay between the molecular conformation and the electronic structure have so far focused on rather large systems (from *n*-butane, 1,3-butadiene, glycine, dimethoxymethane, and stilbene to a variety of organic polymers), and it is exceedingly interesting therefore to learn from the latter study that the simple rotation of one O−H bond in an excessively small molecule can apparently induce highly significant changes in the 1s photoelectron spectrum, in an energy region that is usually regarded as bearing very limited information onto chemical bonds and details of the molecular structure. In line with the latter study, we wish to evaluate on theoretical grounds the potential of EMS in probing the influence of the molecular conformation of ethanol on the shape, topology, and spread of the valence orbitals of this compound.

Ethanol is a most common solvent, an environmental friendly fuel,[10] an important product of fermentation, and an essential component of wine. This is the smallest primary alkanol that exhibits two O−H stretching bands in the IR absorption spectrum, in the gas phase,[11] in inert solvents, or in matrix isolation.[12] The molecular structure of ethanol is most commonly discussed in terms of two stationary points on its potential energy surface, namely, the *anti* and *gauche* conformers (Figure 1), of C_s and C_1 symmetries, respectively. The relative energies and abundances of these two conformers in the gas phase have been subject to some debate.[13−15] The rotational isomerism of ethanol has been experimentally investigated by means of microwave spectroscopy[16,17] or infrared spectroscopy.[18−22] The conformational characteristics of ethanol have also been the subject of many theoretical studies.[20,23−27] From a theoretical viewpoint, accurate calculations of conformational energy differences for molecules that are subject to sizable steric interactions involving electron pairs are deemed to require extensive treatments of electronic correlation, and this certainly much beyond second order. To our knowledge, the most thorough study of stationary points on the potential energy surface of ethanol so far is the Focal Point Analysis by Kahn and Bruice,[28] an approach that combines results obtained with theoretical treatments [HF, MP2, MP3, MP4(SDTQ), CCSD, and CCSD(T)] (ref 29), and Dunning's correlation consistent polarized valence basis sets (cc-pVXZ,[30] with X = D, T, Q, 5, 6) of improving quality, in order to evaluate conformational energy differences at the confines of nonrelativistic quantum mechanics. Specifically, with such an analysis (see also refs 2c, 2f, 5, and 31), one exploits the faster convergence of higher order correlation contributions to energy differences and extrapolates the results to an asymptotically complete basis set, to evaluate energy differences at the level of a benchmark CCSD(T) treatment along with an infinitely large basis set. In their work,[28] Kahn and Bruice also employed the Douglas−Kroll approach[32] for evaluating scalar relativistic effects. As is typical for organic molecules containing only first and second row atoms, these were found to be negligible. These very accurate calculations indicate that, in its equilibrium geometry, the *gauche* conformer of ethanol lies at 46.9 cm^{-1} (0.13 kcal/mol) above the *anti* species, to compare with experimental energy differences of 41.2 ± 5.0 (0.118 kcal/mol),[16] 39.2 (0.112 kcal/mol),[17] and 42 cm^{-1} (0.120 kcal/mol).[19] B3LYP/aug-cc-pVTZ corrections for the change in zero-point vibrational energies are almost insignificant (−0.210 cm^{-1}, that is, −0.0006 kcal/mol).

In the present work, use is made of the results of Kahn and Bruice regarding the relative energies of the C_s and C_1 conformers, to simulate the results of (e, 2e) electron impact ionization experiments on ethanol at high kinetic energies and at room temperature. For this purpose, we resort to a thermostatistical analysis[33] that accounts for internal hindered rotations[34] and to high-level calculations of ionization spectra employing one-particle Green's Function (1p-GF) theory or, equivalently, electron propagator theory,[35] using the formalism of Dyson orbitals[36] and the relationships of these orbitals within the framework of 1p-GF theory with EMS.[2d,37] These Green's Function calculations account for initial and final state correlation effects and for the dispersion therefore of the (e, 2e) ionization intensity into shakeup states relating to electronically excited configurations of the cation.[6] Despite the limitations inherent to spherical averaging over all possible molecular orientations in the gas phase and the limited resolution of the (e, 2e) spectrometers on electron binding energies and momenta, it will be shown that the molecular conformation has a particularly strong influence on the electron momentum distributions that can be experimentally inferred from an angular analysis of the (e, 2e) ionization cross-sections of ethanol.

Theoretical Outline

In the present work, we wish to simulate the outcome of EMS experiments performed using a standard (e, 2e) noncoplanar symmetric kinematical setup and at a high electron impact energy relative to the valence electron energies. We correspondingly invoke the Born approximation, that is, the assumption of a sudden ionization process. We also assume a binary (e, 2e) encounter and, thus, a high electronic momentum transfer and a negligible kinetic energy transfer to the residual cation. We at last assume that the plane wave impulse approximation (PWIA) is valid and express therefore the triple differential EMS cross-section for a given ionization state (*n*) and for randomly oriented molecules as follows:[4]

$$\sigma_n \propto \int d\Omega \left| \langle \nu_{\vec{p}} \Psi_n^{N-1} \Psi_0^N \rangle \right|^2 \qquad (1)$$

with *N* equal to the number of electrons in the molecular target. In the above equation, $\nu_{\vec{p}}$ denotes a plane wave function [exp $(i\vec{p}\cdot\vec{r})$], and $\int d\Omega$ is the integral over the whole solid angle that is required for a spherical averaging of the cross-sections over all possible molecular orientations in the gas phase.

The partial overlaps of the ion and neutral electronic wave functions in eq 1 are referred to as Dyson (spin-) orbitals.[36] Using spin-space coordinates $\mathbf{x} = (\omega, \vec{r})$, these read

$$g_n(\mathbf{x}) = \sqrt{N}\int \Psi_n^{N-1}(\mathbf{x}_1, \mathbf{x}_2, ..., \mathbf{x}_{N-1})\Psi_0^N(\mathbf{x}_1, \mathbf{x}_2, ..., \mathbf{x}_{N-1}, \mathbf{x})\times d\mathbf{x}_1\, d\mathbf{x}_2 ... d\mathbf{x}_{N-1} \quad (2)$$

with N equal to the number of electrons. These orbitals account for both ground-state electronic correlation and dynamical relaxation effects, as well as for the dispersion of the ionization intensity over states relating to excited (shakeup) electronic configurations of the cation: By definition, the norm of a Dyson orbital is thus smaller than one. The (e, 2e) ionization cross-sections are in turn directly proportional to structure factors derived as the Fourier transforms of Dyson orbitals for the ionization channels under consideration:[4]

$$\sigma_n = K\int \left|g_n(\omega, \vec{p})\right|^2 d\Omega \quad (3)$$

where ω and $\vec{p}$ represent the spin and momentum of the electron prior to ionization.

Under a standard symmetric noncoplanar geometrical setup for studying in coincidence the kinematics of (e, 2e) ionization events at high electron impact energies, the (modulus of the) initial momentum of the knocked-out electron (p) can be monitored by scanning the azimuthal angle (ϕ) under which the electrons are selected, according to basic conservation laws on momenta and energies:[4]

$$p = \sqrt{(2p_1\cos\theta - p_0)^2 + [2p_1\sin\theta\sin(\varphi/2)]^2} \quad (4)$$

and

$$E_1 + E_2 = E_0 - E_n = E_{\text{total}} \quad (5)$$

with E_1 (p_1) and E_2 (p_2) the energies (momenta) of the two outgoing electrons ($E_1 = E_2$, $p_1 = p_2$) and where $\theta = \theta_1 = \theta_2 = 45°$ defines the polar angles used in the experiment. In the above equations, E_0 and p_0 stand for the impact energy and momentum of the incoming electron, and E_n is the binding energy (i.e., ionization energy, $IP_n > 0$) of the target electron.

Dyson orbitals are most conveniently expanded as linear combinations of HF orbitals $|\phi_i\rangle$, with Feynman−Dyson transition amplitudes $[x_i^{(n)}]$ as weight coefficients[36]

$$g_n(\mathbf{x}) = \langle\Psi_n^{N-1}|\Psi_0^N\rangle_{N-1} = \sum_i x_i^{(n)}\phi_i(\mathbf{x}) \quad (6)$$

$$x_i^{(n)} = \langle\Psi_n^{N-1}|a_i|\Psi_0^N\rangle,\ \ \forall\, n \in \{N-1\} \quad (7)$$

The norm of the above Dyson orbital (eq 6) related to state $|\Psi_n^{N-1}\rangle$, defines the associated spectroscopic strength ($\Gamma_n < 1$), that is, the probability to observe that state regardless of cross section effects:[38]

$$\Gamma_n = \langle\Psi_n^{N-1}|\Psi_0^N\rangle_{N-1}{}^2 = \sum_i x_i^{(n)2} \quad (8)$$

In the framework of an exact many-body quantum mechanical theory, Feynman−Dyson amplitudes for a given ionic state (n) are obtained[36] from the residues at the poles of the advanced component (A) of the one-particle Green's Function (1p-GF) in the complex energy plane

$$G_{ij}^A(\omega) = \sum_{n\in(N-1)} \frac{x_i^{(n)}x_i^{(n)*}}{\omega + IP_n - iO^+} \quad (9)$$

Obviously, the locations of these poles straightforwardly relate to the corresponding ionization energies (IP_n). In 1p-GF theory, the factors required for renormalizing Dyson orbitals are therefore most customary referred to as pole strengths.[35]

Assuming a depiction of ionization events at the level of Koopmans' theorem, Dyson orbitals most naturally reduce to Hartree−Fock orbitals (target Hartree−Fock approximation, THFA[39]), pole strengths become equal to 1, and ionization energies straightforwardly relate to HF orbital energies, after a change of sign. Most EMS experiments have been empirically interpreted using the target Kohn−Sham approximation (TKSA[40]), which amounts to substituting Dyson orbitals by the most relevant Kohn−Sham orbitals. Although KS orbitals have been most generally providing far more quantitative insights into (e, 2e) electron momentum distributions than their HF counterparts, their physical significance in the context of ionization spectroscopy has been subject to vigorous debates. Kohn−Sham orbitals are traditionally introduced in density functional theory (DFT[41]) as a set of auxiliary mathematical one-electron functions used to expand the ground-state electron density of an ideal noninteracting system, which is then mapped onto the exact density through a minimization of the energy. A standard view expressed in the literature is that in an exact DFT framework only the energy of the highest occupied molecular orbital (HOMO) is known to have a physical meaning as (minus) the vertical ionization energy.[42]

An analogue of Koopmans' theorem in DFT, which approximates (after a change of sign) all KS orbital energies to relaxed ionization energies for primary ionization events and which becomes an exact identity for the HOMO, has been established recently.[43] However, the self-interaction error that is inherent to DFT calculations has prevented widespread applications of the so-called meta-Koopmans theorem[43] with standard hybrid and gradient-corrected exchange-correlation functionals, such as the Becke-three-parameters-Lee−Yang−Parr functional (B3LYP[44]). This error results in a spurious electronic potential in the asymptotic region,[45] and Kohn−Sham orbital energies obtained with standard hybrid GGA functionals like B3LYP are known in general to yield estimates of ionization energies that most commonly underestimate the experimental values by 3−4 eV.[46] Such functionals have been parametrized for computing at best the neutral ground-state electron densities and related properties but certainly not for evaluating transition densities toward ionic states. Unsurprisingly, even upon accounting for the dispersion of the ionization intensity over shakeup states, standard KS orbitals may occasionally significantly differ from Dyson orbitals, in particular when dealing with molecules exhibiting a low symmetry point group and localized lone pair levels[2f] or with electronically excited states,[36e] an observation that motivates further assessment of KS orbitals against benchmark Dyson orbitals and experimental momentum distributions. In the framework of conceptual DFT,[47] Dyson orbitals relate in a rather complicated way to Fukui functions.[48] These were introduced by Parr and Wang[49] as a generalization of Fukui's frontier molecular orbital concept[50] and are defined as electron density derivatives with respect to the total particle number.[47,49] From a mathematical viewpoint, there are thus no straightforward and obvious relationships between Kohn−Sham and Dyson orbitals. Overlap functions like Dyson orbitals are valid for any many-fermions system. It is worth noticing therefore that such functions have been amply used in nuclear physics[51] for studying the properties of quasi-hole states of many-nucleon systems and proton emission following the electron-impact excitation of nuclei in (e, e′p) experiments.

Computational Details

All computations that are discussed in the present work are based on molecular geometries that have been optimized by

means of DFT calculations employing the B3LYP functional and Dunning's aug-cc-pVTZ basis set (correlation consistent polarized valence basis set of triple-ζ quality,[30a] augmented by a set of *s*, *p*, and *d* diffuse functions on hydrogens and of *s*, *p*, *d*, and *f* diffuse functions on the carbon and oxygen atoms[30a]). The main motivation for this choice is that the B3LYP approach in conjunction with large enough basis sets is known[52] to provide equilibrium structures, vibrational, and, thus, thermochemical properties at a level of accuracy equivalent to that reached with the benchmark CCSD(T) level (Coupled Cluster Ansatz upon single and double electronic excitations and augmented by a perturbative estimate of triple excitations).

The relative abundances of the C_1 and C_s conformers of ethanol have been calculated using Boltzmann's thermostatistics:

$$n_i = \rho_i e^{-\Delta G_i/RT} \tag{10}$$

with ρ_i a factor equal to the multiplicity (or symmetry number) of the species of interest [1 for the *anti* (C_s) conformer, and 2 for the *gauche* (C_1) conformer]. Here, ΔG_i denotes our best estimate for the Gibbs free energy difference between the two conformers, which was obtained by adding to the FPA estimates by Kahn and Bruice[28] of the *gauche*−*anti* energy difference the B3LYP/aug-cc-pVTZ corrections for zero-point vibrational energies and thermal contributions to the enthalpies, as well as entropy contributions. The thermochemical analysis that is presented here goes beyond a standard treatment based on the rigid rotor−harmonic oscillator (RRHO) approximation: The employed partition functions account for hindered rotations, according to the protocol by Ayala and Schlegel[34] for identifying and treating the internal rotation modes, the protocol by Kilpatrick and Pitzer[53] for calculating the kinetic energy matrix describing the internal rotations, as well as the rules by Mayo, Olafson, and Goddard[54] for defining the potential periodicity, the rotating tops' symmetry numbers, and the well-multiplicities of acyclic molecules. The employed procedure also incorporates an improved analytical approximation, according to a best-fit procedure, of the formula of Pitzer and Gwinn[55] for the partition function associated with one-dimensional hindered internal rotations. All DFT and related thermochemical calculations presented in this work have been performed using the GAUSSIAN03 package of programs.[56]

Valence one-electron and shakeup ionization spectra as well as the related Dyson orbitals have been computed by means of one-particle Green's Function (or electron propagator) theory,[35] along with the so-called third-order algebraic diagrammatic construction [ADC(3)] scheme.[57] With such an approach, calculating vertical ionization energies (or vertical electron attachment energies) implies solving a secular problem of the form $\mathbf{HX} = \mathbf{XE}$ (with $\mathbf{XX}^\dagger = \mathbf{1}$), in which the secular Hamiltonian matrix ($\mathbf{H}$) to diagonalize is cast over cationic ($N - 1$) or anionic ($N + 1$) electronic states comprising, for the cationic states, primary one-hole ($1h$) and singly excited two-hole−one-particle ($2h1p$) shake-up states, and correspondingly for the anionic states, one-particle ($1p$) and singly excited two-particle−one-hole ($2p1h$) shake-on states. Coupling amplitudes between the $N + 1$ and the $N - 1$ states identically vanish in a treatment of one-electron ionization energies that is correct through third-order in electronic correlation. At the 1p-GF/ADC(3) level, the $\mathbf{H}$ matrix has therefore a block-diagonal structure comprising $1h$-$1h$ ($1p$-$1p$), $2h1p$-$1p$ ($2p1h$-$1h$), and $2h1p$-$2h1p$ ($2p1h$-$2p1h$) matrix elements that are expanded through fourth-order and at second- and first-order in electronic correlation, respectively. The ADC(3) scheme enables calculations of one-electron ionization energies at a level of accuracy (∼0.2 eV), which is comparable to that reached with the multireference single-double configuration interaction (MR-SDCI) scheme (see ref 58 and references therein), with the key advantages of size consistency and of a greater compactness of the secular matrix to diagonalize. Singly excited $2h1p$ ($2p1h$) states are correspondingly described through first-order only, which implies a lower accuracy on shakeup ionization energies, typically around ∼0.6 eV. In both cases, the Feynman−Dyson transition amplitudes [$x_i^{(n)}$] required to expand the related Dyson orbitals and spectroscopic strengths are obtained[2d,37] as the $1h+1p$ components of the associated eigenvectors (X_{in}).

The 1p-GF/ADC(3) calculations have been performed under the assumption of frozen core electrons, using the original package of programs interfaced to GAMESS,[59] and resorting to the band Lanczos diagonalization approach[60] for projecting the $2p$-$1h$ shake-on states onto a pseudoelectron attachment spectrum, prior to a complete diagonalization of the so reduced $\mathbf{H}$ matrix, this time by means of the block-Davidson approach.[61] All eigenstates with a pole strength larger or equal to 0.02 have been recovered up to electron binding energies of 30 eV. At the SCF level, the requested convergence on the elements of the one-electron density matrix was set equal to 10^{-10}. The symmetry point group of the C_s conformer of ethanol has been exploited. Two basis sets have been employed in these ADC(3) calculations: cc-pVDZ (Dunning's correlation consistent polarized valence basis set of double-ζ quality[30a]) and cc-pVDZ++. The latter was implemented by deleting the *d* type diffuse functions on the oxygen and carbon atoms in the aug-cc-pVDZ basis set, to overcome severe linear dependencies resulting in a divergence at the level of the evaluation of the static self-energy. The cc-pVDZ++ basis set incorporates, therefore, *s* and *p* diffuse functions on the hydrogen, carbon, and oxygen atoms.

Thermally averaged ADC(3) ionization spectra will be presented in the sequel as spike and convoluted spectra, using as a convolution function a Voigt profile combining a Gaussian and a Lorentzian with equal weight and a constant full width at half-maximum parameter of 0.4 or 1.1 eV, respectively. These parameters have been selected to enable comparisons with available measurements performed using UPS (HeI) or EMS. In these simulations, line intensities have been scaled according to the computed spectroscopic strengths (Γ_n) or (e, 2e) cross-sections, respectively, along with the relative conformer abundances.

Thermally and spherically averaged Dyson orbital momentum distributions at specific electron binding energies have been correspondingly computed according to the formalism described in the preceding section, taking into account the influence of the molecular conformation onto the orbital ionization energies and assuming a symmetric noncoplanar kinematics and an electron impact energy (E_0) of 1200 eV (+ electron binding energy, E_n). Therefore, the relevant parameters for the momenta of the impinging and outgoing electrons amount to $p_0 = 0.271105\ (1200 + E_n)^{1/2}$ au (1 au = 1 a_0^{-1} with a_0 the Bohr radius, i.e., 0.5292 Å), and $p_1 = p_2 = 6.64077$ au, respectively ($E_1 = E_2 = 600$ eV). Our calculations of momentum distributions and of spherically averaged (e, 2e) cross-sections also account for a limited resolution of $\Delta\phi = \pm 0.84°$ and $\Delta\theta = \pm 0.57°$, which implies a momentum resolution of $\Delta p \sim 0.16$ (fwhm) or 0.069 au (one standard deviation) at an impact energy of 1.2 keV. These parameters are consistent with the characteristics of a newly developed (e, 2e) spectrometer[62] at Tsinghua University (Beijing, China). In the present work, the limited

TABLE 1: Structural Parameters of Ethanol[a]

structural parameters	experiment[b]		B3LYP/aug-cc-pVTZ[c]	
	C_1	C_s	C_1	C_s
C_1-C_2	1.512(3)	1.499(3)	1.52	1.51
C_2-O_3	1.422(2)	1.431(2)	1.43	1.43
O_3-H_4	0.85(3)	0.79(4)	0.96	0.96
C_1-H_5	0.96(4)	0.93(3)	1.09	1.09
C_1-H_6	1.05(4)	1.01(3)	1.09	1.09
C_1-H_7	1.01(3)	0.95(3)	1.09	1.09
C_2-H_8	1.04(3)	0.96(3)	1.07	1.10
C_2-H_9	0.93(3)	0.98(3)	1.09	1.10
$C_1-C_2-O_3$	112	108.8	113.0	108.1
$C_2-O_3-H_4$	102	107	108.9	109.1
$H_5-C_1-C_2$	115	113	110.6	110.4
$H_6-C_1-C_2$	113	114	111.1	110.6
$H_7-C_1-C_2$	109	109	110.7	110.6
$H_8-C_2-C_1$	107	115	110.4	110.2
$H_9-C_2-C_1$	118	117	110.4	110.2
$H_8-C_2-O_3$	110	112	110.3	110.3
$H_9-C_2-O_3$	104	109	105.0	110.3
$C_1-C_2-O_3-H_4$	63 ± 2	179 ± 2	61.7	180.0
$H_5-C_1-C_2-O_3$			177.6	180.0
$H_6-C_1-C_2-O_3$			−63.0	−59.95
$H_7-C_1-C_2-O_3$			+57.3	+59.95

[a] All bond lengths and angles are in Å and degrees, respectively. [b] Uncorrected X-ray diffraction data, taken from ref 64. [c] This work.

resolution in momentum has been accounted for by means of a procedure employing Monte Carlo simulations.[63]

Results and Discussion

Molecular Structures and Relative Conformer Abundances. The employed molecular geometries for the *trans* (C_s) and *gauche* (C_1) conformers are given through the interplay of Figure 1 and Table 1. In spite of the polarity of the target molecule (ethanol) and of strong intermolecular interactions in the solid phase, therefore, the agreement between theoretical results with X-ray diffraction data[64] is as good as it could be. Deviations on bond lengths and bond or torsion angles are in general around 0.02 Å and a few degrees. The largest discrepancies are between encountered for the O_3-H_4 bond length and for the $C_2-O_3-H_4$ bond angle in the C_1 conformer. Note that the C_1 and C_s conformers differ precisely by the rotation of the O_3-H_4 bond around the C_2-O_3 bond. Despite the very shallow nature of the related torsion potential, solid state effects apparently have a limited influence on the $H_4-O_3-C_2-C_1$ dihedral angle of the C_1 species (Table 1).

As with any ionization experiment performed under high vacuum conditions, it is in practice extremely hard to monitor the temperature at which the (e, 2e) ionization events occur. The vapor sample may substantially cool down because of a merely adiabatic gas expansion. We wish to note therefore that the enthalpy and entropy corrections both have a very limited influence on the conformer weights and that these in turn do not vary by more than ∼3.5% upon an increase of the temperature from 198.15 to 398.15 K (Table 2). At 298.15 K, thermal corrections to the enthalpy of the *gauche* (C_1) conformer vs the reference *trans* (C_s) species amount to −0.01(2) kcal/mol only. Added to the best FPA estimate for the electronic energy difference [ΔE = 0.13(4) kcal/mol], this yields an enthalpy difference between the two conformers of ∼0.12(2) kcal/mol (zero-point vibrational energies included). The corresponding entropy variation (ΔS) at room temperature amounts to −0.068 cal mol^{-1} K^{-1} at the RRHO level and to −0.116 cal mol^{-1} K^{-1} upon accounting for hindered rotations, yielding

TABLE 2: Boltzmann Statistical Thermodynamical Calculations of Conformer Abundances at the RRHO Level and upon Accounting for Hindered Rotations

	hindered rotations		RRHO	
temperature (K)	C_1 (%)	C_s (%)	C_1 (%)	C_s (%)
198.15	58.5	41.5	58.9	41.1
223.15	59.2	40.8	59.7	40.3
248.15	59.8	40.2	60.4	39.6
273.15	60.3	39.7	60.9	39.1
298.15	60.7	39.3	61.3	38.7
323.15	61.1	38.9	61.7	38.3
348.15	61.4	38.6	62.0	38.0
373.15	61.8	38.2	62.3	37.7
398.15	62.0	38.0	62.5	37.5

Gibb's free energy differences of +0.14(1) or +0.15(7) kcal/mol, respectively. Because the two conformers are almost isoenergetic, according to the work by Kahn and Bruice, the conformer abundances merely reflect the symmetry numbers (Table 2). Note also that as compared with RRHO calculations, accounting for the influence of hindered rotations has only a marginal effect on these abundances. According to our best estimates, the equilibrium mixture of ethanol at room temperature is therefore characterized by *gauche* (C_1) and *anti* (C_s) molar fractions that are equal to 0.607 and 0.393, respectively. Shaw et al.[26] obtained correspondingly molar fractions of 0.612 and 0.388 from a fitting of theoretical IR spectra with experimental measurements in highly diluted CCl_4 solutions. Very similar values (0.62 vs 0.38) can be inferred from the energy data by Kakar et al.[16] or Pearson et al.[17]

Valence Electronic Structure and Ionization Spectra. In the *gauche* (C_1) conformer, due to the lack of any symmetry, there is no restriction at all on the way atomic orbitals may mix, and the greatest care is needed therefore to establish a correlation diagram with the molecular orbitals of the *anti* (C_s) conformer. Molecular orbital correlation diagrams between these two conformers were obtained (Figures 2 and 3) by carefully studying the evolution of the orbital energies in the outer- and inner-valence regions as a function of the $H_4-O_3-C_2-C_1$ dihedral angle (ϕ). Somewhat counterintuitively, this geometrical parameter has almost no influence on the energy of the three outermost orbitals, among which the 3a″ (C_s) alias 13a (C_1) and the 10a′ (C_s) alias 12a (C_1) lone-pair levels. The influence on the C_{2s} and O_{2s} inner-valence levels is also rather limited and does not exceed 0.3 eV. Very significant variations are on the other hand observed for orbitals in the middle of the outer-valence ($C_{2p} + O_{2p} + H_{1s}$) region. The 8a′ orbital of the *anti* conformer [shortly 8a′ (C_s)] gets stabilized by ∼1 eV when becoming the 9a orbital of the *gauche* conformer [shortly 9a (C_1)], as a result of a release of through space antibonding interactions between the O−H bond and the methyl group. On the contrary, a destabilization by almost 0.6 eV is correspondingly noted for the 1a″ (C_s) orbital, due to the disruption of through-space bonding interactions (Figure 2) between the methyl group and the n_π(O) lone pair upon a twist in the *gauche* conformation. Because electron momentum distributions are experimentally reconstructed from an angular analysis of (e, 2e) ionization intensities at specific electron binding energies, it will clearly be essential to account for the influence of the molecular conformation on electron binding energies, to correctly unravel EMS experiments on ethanol. Any study that would neglect this influence should be regarded as physically irrelevant.

The thermally averaged and convoluted ADC(3) spectra displayed in Figure 4 reflect the partition of the valence

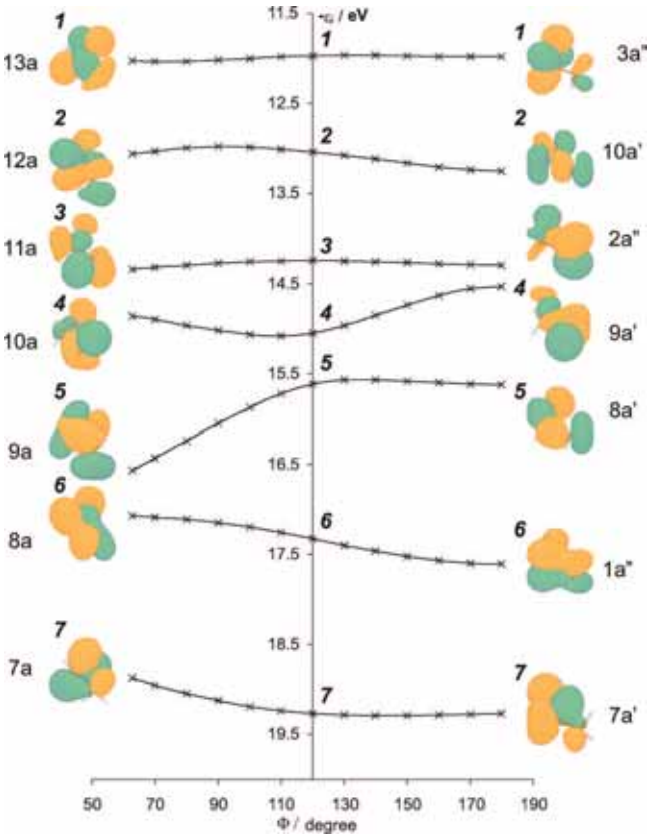

Figure 2. Molecular orbital correlation diagram for the outer valence region as a function of the dihedral angle Φ ($H_4-O_3-C_2-C_1$). HF/cc-pVDZ++ results upon B3LYP/aug-cc-pVTZ geometries.

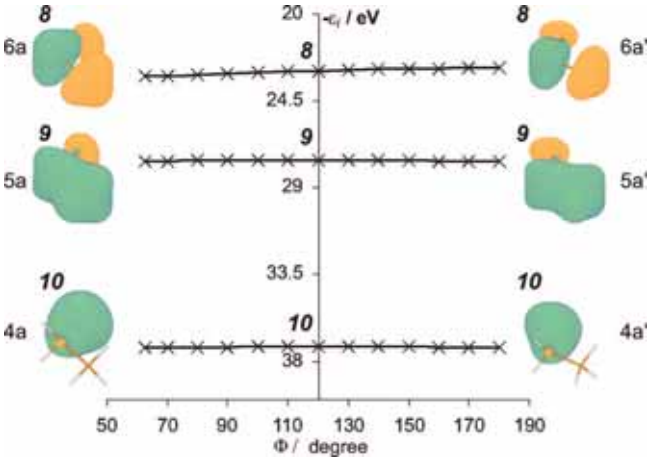

Figure 3. Molecular orbital correlation diagram for the inner valence region as a function of the dihedral angle Φ ($H_4-O_3-C_2-C_1$). HF/cc-pVDZ++ results upon B3LYP/aug-cc-pVTZ geometries.

electronic structure into three inner-valence levels and seven outer-valence levels at electron binding energies above and below ~19 eV, respectively. The individual conformer contributions to the ionization spectrum are also provided, in the form of spike spectra. The reader is referred to Table 3 for a detailed assignment of these spectra and to Figure 5 for a comparison with the experimental HeI measurements by Katsumata et al.[65] According to our simulations, a rather pronounced shoulder (V) at ~14.5 eV in this ultraviolet photoelectron spectrum specifically relates to the 8a′ (C_s) orbital and may therefore be regarded as a rather reliable conformational fingerprint. The rather significant influence of the molecular conformation onto ionization energies at electron binding energies between 15 and 18 eV also explains the larger widths that characterize bands VI and VII in the UPS measurements. When accounting for conformational effects, the ADC(3) calculations enable overall theoretical insights in the available one-electron experimental energies within ~0.2 eV accuracy, to compare with an accuracy of only 1.1 eV at the level of theory (HF/4-31G) that was employed by Katsumata et al.[65] for assigning their measurements. Note that, to our knowledge, no calculations of the ionization spectrum of ethanol beyond the level of Koopmans' theorem have been reported so far. Table 3 confirms also that an application of the meta-Koopmans' theorem onto B3LYP Kohn−Sham orbital energies leads to underestimations of one-electron ionization energies of the order of 3−4 eV, as compared with the available experimental values.

A breakdown of the orbital picture of ionization is noted at electron binding energies larger than 24 eV. Except for a redistribution of shakeup intensities in this energy region, the computed ionization spectrum is from a qualitative viewpoint almost insensitive to the incorporation of diffuse functions in the cc-pVDZ basis set. The influence of these functions on the one-electron binding energies does not exceed ~0.2 eV. The vertical double ionization threshold is located at ~29.9 eV according to CCSD(T)/aug-cc-pVTZ calculations, which explains the very strong influence of diffuse functions on the shakeup splitting in the O_{2s} electron binding energy range [~31 to ~34 eV, according to ADC(3) results]. Because for this energy range a second electron is subject to decay in the continuum, the computed shakeup states should rather be regarded as discrete approximations to a continuum of shake-off resonances. Because of the imposition of a threshold of 0.02 on spectroscopic strengths during the search for eigenstates of the ADC(3) secular matrix, a much lower fraction of the O_{2s} ionization intensity is recovered at the ADC(3)/cc-pVDZ++ level.

Simulations of thermally and spherically averaged (e, 2e) ionization spectra at room temperature are provided in Figure 6, along with the individual conformer contributions and the underlying spike (e, 2e) ionization spectra, at an electron impact energy of 1.2 keV and at azimuthal angles ranging from 0 to 10 degrees. The selected fwhm parameter (1.1 eV) for the employed spread function qualitatively accounts both for the combined effect of natural and vibrational broadening (~0.6 eV, as estimated from the UPS measurements) and for the energy resolution (~0.5 eV) of the best experimental EMS set ups to date. Despite the very strong influence of the molecular conformation on the (e, 2e) ionization spectra, these simulations indicate that seven bands remain visible at all selected azimuthal angles and are therefore suited for a detailed EMS study of the interplay of the electronic wave function with the molecular structure of ethanol.

Because of the lack of symmetry constraints, all molecular orbitals of the C_1 conformer significantly contribute to (e, 2e) ionization intensities at $\phi = 0°$. In contrast, note that the contribution to band 1 at 10.9 eV of the C_s conformer (10.9 eV) vanishes at $\phi = 0°$ and becomes increasingly significant at increasing values of the azimuthal angle, a behavior that is typical of a p type electron momentum distribution. This behavior is consistent with the antisymmetric nature of the HOMO in the C_s conformer and the presence in this orbital of three mutually perpendicular nodal planes (Figure 2). Because of particularly large ionization cross-sections associated with the minor C_s conformer fraction, two bands (2 and 5) strongly protrude at electron binding energies of 12.4 and 17.8 eV and tend to disappear at larger azimuthal angles. At $\phi = 0°$, the C_s

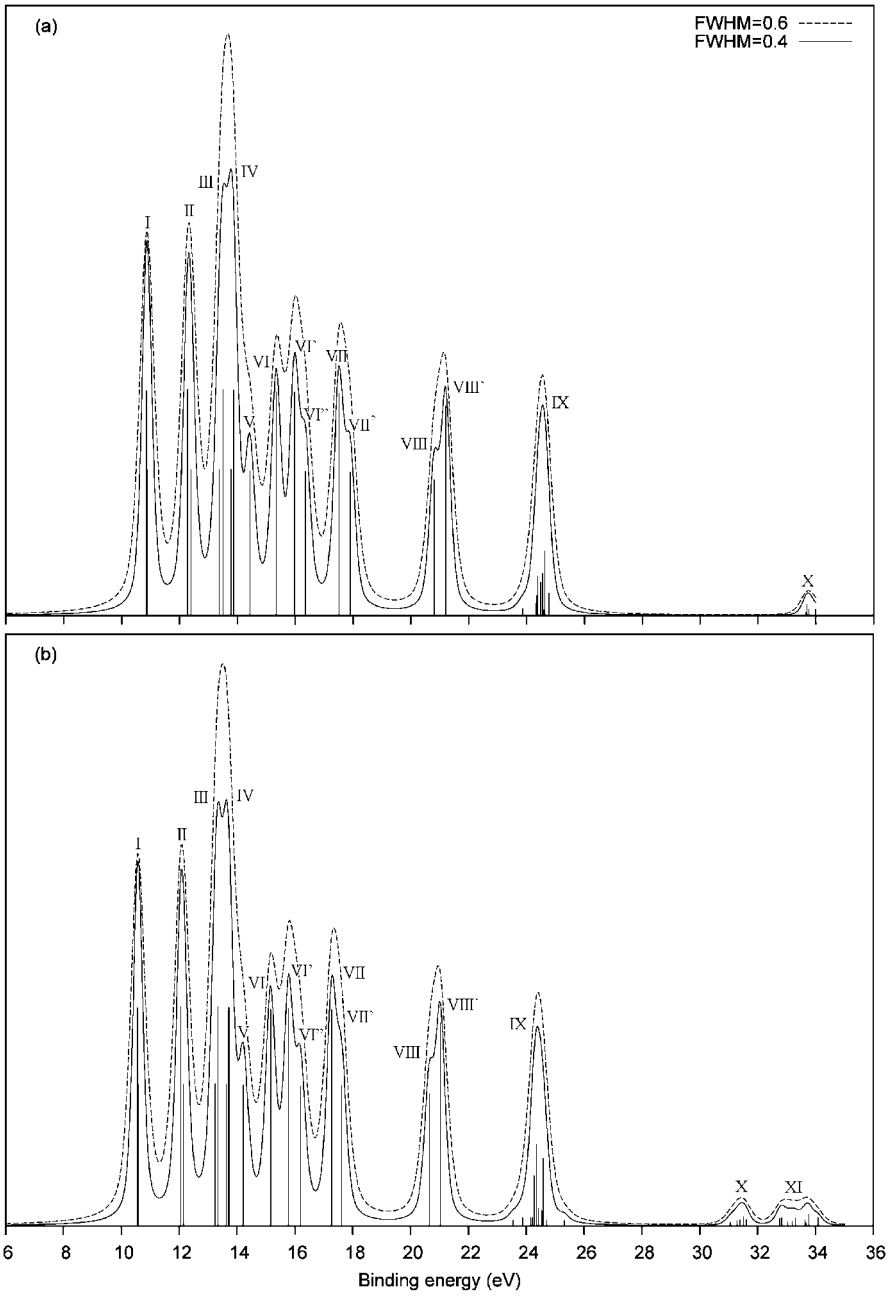

Figure 4. Thermally averaged ($T = 298.15$ K) 1p-GF/ADC(3) ionization spectra of ethanol (full line: fwhm = 0.4 eV, dashed line: fwhm = 0.6 eV); (a) ADC(3)/cc-pVDZ++ and (b) ADC(3)/cc-pVDZ results.

and C_1 conformers provide maximal and marginally small contributions to these bands, respectively, whereas at the largest azimuthal angles, these contributions become approximately proportional to the conformer abundances. This observation is already indicative of a particularly strong conformational fingerprint in the associated momentum distributions, which is predicted to be of the *s* type (see further). In sharp contrast with bands 2 and 5, bands 3 and 4 at electron binding energies of 13.6. and 15.8 eV dominantly relate to the C_1 conformer at low azimuthal angles. For the latter band, the contribution to band 4 of the C_s conformer remains comparatively quite limited even at the largest values of ϕ. The respective contributions of the C_s and C_1 conformers to the outermost C_{2s} band (6) at 21.0 eV merely reflect their abundances. Because of the release of symmetry constraints upon configuration interactions in the final ionic state and an increased shakeup splitting therefore upon lowering the symmetry from C_s to C_1, the contributions of the *anti* and *gauche* conformers to band 7 are accidentally almost equal. This relates to the fact that, because of an imposed threshold of 0.02 on the recovered ADC(3)/cc-pVDZ++ spectroscopic strengths, only 69.6 and 67.3% of the ionization intensity associated to the innermost C_{2s} level could be recovered for the C_s and C_1 conformers, respectively. Most generally, except for an enhanced shakeup fragmentation with no significant alteration of the computed spectral envelope, [66] innermost valence ionization bands are known in general to bear no experimentally amenable information on the molecular conformation.[1]

Electron Momentum Distributions. Thermally and spherically averaged electron momentum distributions for each resolvable one-electron ionization band (1−6) in the (e, 2e) spectra displayed in Figure 6 are provided at various theoretical levels in Figure 7 and compared with experimental results at an electron impact energy of 1.2 keV from the (e, 2e) research

TABLE 3: Comparison of Theoretical Ionization Spectra with UPS Measurements[a]

orbital labels	HF/aug-cc-pVDZ	B3LYP/aug-cc-pVDZ	ADC(3)/cc-pVDZ	ADC(3)/cc-pVDZ++	UPS/He I[b] exp.	UPS peak[b]	EMS peak[d]
13a (C_1)	12.048	7.645	10.571 (0.913)	10.861 (0.911)	10.64	I	1
3a″ (C_s)	12.006	7.604	10.587 (0.915)	10.887 (0.913)			
12a (C_1)	13.100	9.048	12.056 (0.918)	12.279 (0.916)	12.18	II	2
10a′ (C_s)	13.296	9.221	12.151 (0.915)	12.392 (0.914)			
2a″ (C_s)	14.270	10.062	13.242 (0.917)	13.372 (0.915)	13.21	III	3
11a (C_1)	14.281	10.248	13.348 (0.917)	13.513 (0.915)			
9a′ (C_s)	14.493	10.541	13.621 (0.916)	13.770 (0.915)	13.86	IV	3
10a (C_1)	14.820	10.557	13.720 (0.914)	13.865 (0.912)			
8a′ (C_s)	15.512	11.094	14.222 (0.910)	14.431 (0.907)	14.50	V	3
9a (C_1)	16.484	11.884	15.161 (0.907)	15.343 (0.905)	15.85	VI	4
8a (C_1)	16.926	12.480	15.786 (0.909)	15.973 (0.906)		VI′[c]	
1a″ (C_s)	17.513	12.774	16.196 (0.904)	16.354 (0.901)		VI″[c]	
7a (C_1)	18.665	13.834	17.274 (0.903)	17.508 (0.900)	17.35	VII	5
7a′ (C_s)	19.000	14.213	17.622 (0.904)	17.901 (0.901)		VII′[c]	
6a′ (C_s)	22.745	16.774	20.646 (0.852)	20.800 (0.849)		VIII[c]	6
6a (C_1)	23.116	17.172	21.032 (0.850)	21.204 (0.848)		VIII′[c]	
5a (C_1)	27.593	20.535	24.279 (0.211)	24.477 (0.135)		IX[c]	7
			24.584 (0.285)	24.632 (0.263)			
5a′ (C_s)	27.598	20.553	24.356 (0.525)	24.386 (0.248)			
			24.536 (0.101)	24.549 (0.266)		IX[c]	7
				24.639 (0.182)			
4a′ (C_s)	36.932	27.892					
4a (C_1)	36.949	27.910					

[a] Binding energies are given in eV, along with spectroscopic strengths (or pole strengths, Γ_n) in parentheses. The last two entries refer to the band assignment in the spectra displayed in Figures 4−6, respectively. Additional ADC(3)cc-pVDZ shake-up lines. 5a(C_1): 23.556(0.025), 23.877(0.034), 24.156(0.035), 24.413(0.073), 24.547(0.032), and 24.711(0.025). 5a′(C_s): 24.211(0.054), 24.707(0.038), and 25.310(0.036). ADC(3)cc-pVDZ lines beyond the double ionization threshold. 4a(C_1): 32.774(0.034) and 32.837(0.036). 4a′(C_s): 31.049(0.022), 31.073(0.021), 31.294(0.036), 31.383(0.039), 31.510(0.059), 31.614(0.044), 33.045(0.028), 33.199(0.028), 33.307(0.049), 33.633(0.039), 33.673(0.021), 33.773(0.077), and 34.089(0.053). Bands X and group of bands XI. Additional ADC(3)cc-pVDZ++ shake-up lines. 5a (C_1): 23.862(0.029), 24.334(0.048), 24.346(0.082), 24.599(0.024), and 24.767(0.092). ADC(3)cc-pVDZ++ lines beyond the double ionization threshold. 4a′(C_s): 33.661(0.021), 33.700(0.072), 33.757(0.039), and 33.991(0.041). Band X. [b] See ref 65b. [c] Our assignment. See the ADC(3)/cc-pVDZ++ simulation displayed in Figure 4. [d] Our assignment. See ADC(3)/cc-pVDZ++ simulations displayed in Figure 6.

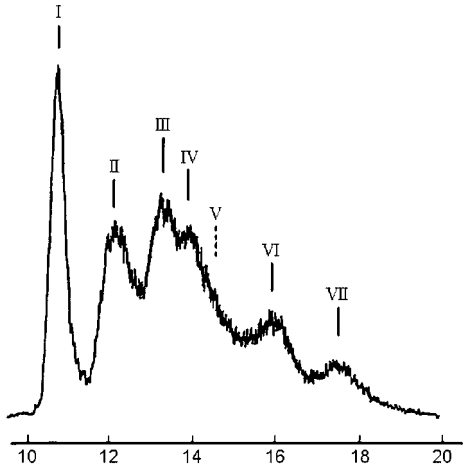

Figure 5. Experimental He I UPS spectrum.[65b]

group at Tsinghua University. Details of this experimental study will be provided in a separate contribution, along with measurements at various electron impact energies[67] to assess the validity of the PWIA.

In line with the proposed assignment for the (e, 2e) ionization spectra (Table 3), these experimental momentum distributions have been analyzed using a C_1/C_s conformer ratio of 0.607/0.393 and according to the following sets of orbitals: {13a(C_1), 3a″(C_s)}, {12a (C_1), 10a′(C_s)}, {2a″(C_s), 11a(C_1), 9a′(C_s), 10a(C_1), 8a′(C_s)}, {9a(C_1), 8a(C_1), 1a″(C_s)}, {7a(C_1), 7a′(C_s)}, and {6a′(C_s), 6a(C_s)}, respectively. In our analysis, we thereby account for the extremely strong influence of the molecular conformation on the energy of the 8a′(C_s) vs the 9a(C_1) orbitals, which are found to contribute to the electron momentum distributions associated to bands 3 and 4, respectively. We note from Table 3 that the spectroscopic strengths (Γ_n) of the one-electron ionization lines that contribute to these outer- and inner-valence ionization bands smoothly decrease from 0.91 to 0.85 with increasing electron binding energies and must be accounted for, therefore, in a quantitative analysis of EMS momentum distributions, within a few percents accuracy.

These spectroscopic strengths are straightforwardly included in an analysis employing Dyson orbitals (see eq 6). On the contrary, Kohn−Sham orbitals are by construction normalized and must be rescaled according to suitable values of the spectroscopic strengths to account for the dispersion of the ionization intensity over 2*h*-1*p* shakeup satellites and correlation bands. The limited angular resolution of the (e, 2e) spectrometer may significantly alter the apparent electron momentum distributions and must also be folded into these distributions to enable a quantitative analysis of the experimental (e, 2e) ionization intensities, in particular those obtained at low electron momenta. A last difficulty is that experimental (e, 2e) ionization intensities are obtained as (arbitrary) electron counts. Lacking any clue about what an absolute "detector unit" is, a quantitative comparison with theoretical data implies therefore a rescaling of the experimental intensities that must also account for both the limited resolution on electron momenta and the dispersion of the ionization intensity into shakeup sets at high electron binding energies (in this case, $E_n > 26$ eV). In these purposes, the experimental (e, 2e) ionization cross-sections that are provided in Figure 7 have been rescaled onto resolution folded theoretical momentum distributions that were derived from ADC(3) Dyson orbitals ($\Gamma_n < 1$, see eqs 6 and 8), using a global rescaling factor obtained from a least-squares fit over the momentum distributions associated to the one-electron ionization

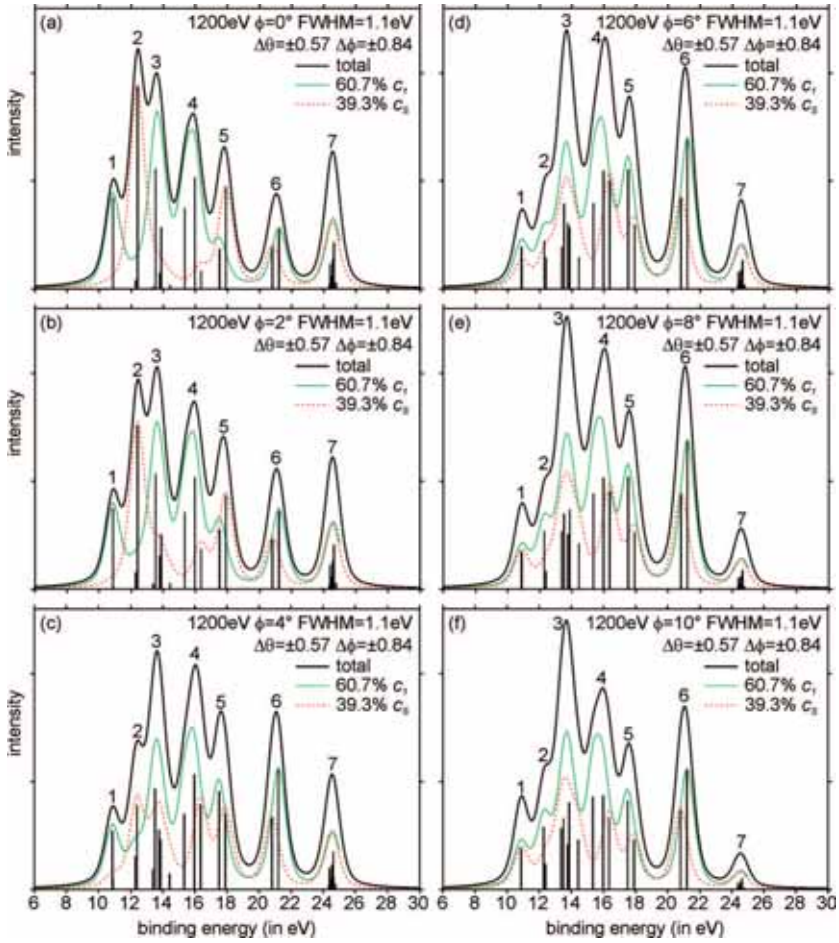

Figure 6. Simulations of spherically and thermally averaged (e, 2e) ionization spectra at $T = 298.15$ K, at $E_0 = 1200$ eV, and at various azimuthal angles: (a) $\phi = 0°$, (b) $\phi = 2°$, (c) $\phi = 4°$, (d) $\phi = 6°$, (e) $\phi = 8°$, and (f) $\phi = 10°$. The full width at half maximum (fwhm) parameter for the Voigt profile was set to 1.1 eV. These spectra were convolved assuming angular resolutions of $\Delta\theta = \pm 0.57°$; $\Delta\phi = \pm 0.84°$ in the (e, 2e) spectrometer (noncoplanar symmetric kinematics).

bands (1−6) at azimuthal angles $\phi = 0$, 2, 4, 6, 8, and 10°. To enable a physically meaningful comparison with experiment that accounts for the same effects, the Kohn−Sham B3LYP orbital momentum distributions that are provided in Figure 7 have also been individually rescaled using the corresponding ADC(3)/cc-pVDZ++ pole strengths. All of our calculations seemingly provide qualitatively consistent insights into the experimental momentum distributions, an observation that motivates first a detailed discussion of the influence of the molecular conformation on these distributions.

To avoid a too severe overcrowding in the computed momentum distributions, we provide separately in Figure 8 the individual orbital contributions that were computed at the ADC(3)/cc-pVDZ++ level, which we compare once more with suitably rescaled experimental momentum distributions, using the above receipes for intensity rescaling. In this figure, these contributions also account for the relative weight of the associated conformer. As expected, inspection of this figure confirms the exceedingly strong influence of the molecular conformation on the (e, 2e) ionization cross-sections and the related EMS momentum distributions. In line with our discussion of the dependence of the (e, 2e) ionization intensities onto the azimuthal angle, examination of Figure 8 confirms the *p* type characteristics of the 3a″ (HOMO), 9a′ and 1a″ orbitals of the C_s conformer, as well as the 12a orbital of the C_1 conformer, an observation that is consistent with the presence of an odd number (1 or 3) of nodal surfaces in all of these orbitals. In contrast, the momentum distributions characterizing the HOMO (13a) of the C_1 conformer and the 10a′ orbital of the C_s conformer exhibit two maxima and one minima, which is in line with the symmetric nature of the 10a′(C_s) orbital or the presence in both cases of two approximately parallel nodal surfaces in these orbitals. As was observed in works on glycine [2a and b], *n*-butane [2c], dimethoxymethane [2f] and *n*-pentane [5], it appears therefore that spherically averaged and resolution folded electron momentum distributions can be significantly influenced by changes in the topology of molecular orbitals, which straightforward reflect in this case alterations thereby of through-space (anomeric) interactions between the oxygen lone-pairs and the nearby methyl group. With ethanol, this effect is particularly impressive, since it relates to the energetically very insignificant OH bond rotation.

The electron momentum distribution characterizing the C_{2s} shakeup band at ∼24.5 eV is analyzed in Figure 9. In line with experiment, all employed models provide essentially the same *s* type electron momentum distributions, and all shakeup lines yield individually the same profile, regardless of the absolute intensity scale. Theory also enables highly quantitative insights into the one-electron momentum distributions recovered from bands 5 and 6 (Figure 8e,f).

In spite of all our efforts, the agreement between our best computations and experiment for the four outermost bands (Figure 8a−d) remains somehow rather deceiving, at least from a quantitative viewpoint. The stronger the influence of the

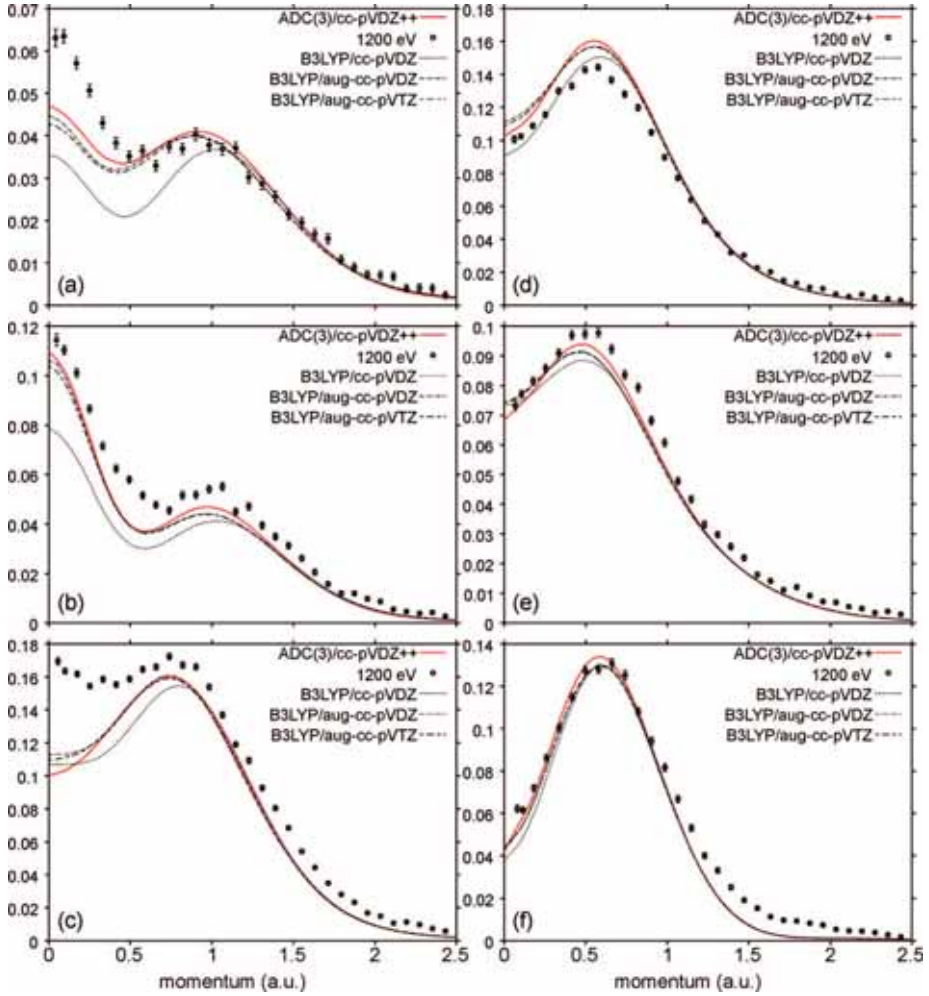

Figure 7. Spherically and thermally averaged electron momentum profiles ($T = 298.15$ K) at various levels of theory as compared with experiment ($E_0 = 1.2$ keV): (a) band 1 ($\epsilon_b \approx 10.9$ eV), (b) band 2 ($\epsilon_b \approx 12.4$ eV), (c) band 3 ($\epsilon_b \approx 13.6$ eV), (d) band 4 ($\epsilon_b \approx 15.8$ eV), (e) band 5 ($\epsilon_b \approx 17.8$ eV), and (f) band 6 ($\epsilon_b \approx 21.0$ eV).

molecular conformation is, the stronger the discrepancy is. It is, however, clear from Figure 8 that a better fit of the experimental momentum distributions cannot be globally improved by using other conformer ratios. The experimental momentum distribution recovered from band 1 can for instance be perfectly fitted by theoretical momentum distributions upon assuming a C_1 to C_s conformer ratio of 0.80 to 0.20, but this would clearly occur at the expense of a strong deterioration of the agreement between theory and experiment for all of the other bands. One may of course be tempted to use or assume variable conformer weights for improving the fitting band per band. Such an analysis would imply that geometrical relaxation effects are rapid enough to induce alterations of the molecular conformation that can be detected in EMS experiments. However, with regards to the kinetic energy of the impinging electron ($E_0 = 1.2$ keV), the time scale characterizing the electron−molecule interaction in EMS is typically of the order of the femtosecond and thus much shorter than that required for nuclear motions in the absence of complications like vibronic coupling interactions or conical intersections between various electronic states. Ethanol has abelian symmetry and does not exhibit any significant near-degeneracies between orbital energies. It is therefore unlikely that these discrepancies between theory and experiment can be ascribed to nuclear dynamical complications in the final cationic states. In other words, ionization processes are expected to be vertical in nature, in which case EMS can only provide instantaneous snapshots of the conformer distributions that statistically prevail in the ground state and which should thus remain constant, whatever the investigated range of electron binding energies. In the next step of our analysis, it is therefore natural to wonder whether the computed momentum distributions are accurate enough. To examine this issue, we now return to Figure 7.

Upon examining the B3LYP momentum distributions that are provided in this figure, it is immediately apparent that, in sharp contrast with the underlying ionization spectrum, diffuse functions have a very significant influence on all of the computed momentum distributions. The effect is particularly pronounced for the momentum distributions to be recovered from the outermost and second ionization bands at 10.9 and 12.4 eV, which is in line with the lone-pair nature of the contributing orbitals. When suitably large enough basis sets are used, it is also clear in this case that B3LYP Kohn−Sham orbitals and ADC(3) Dyson orbitals produce almost equal electron momentum distributions. Note furthermore that at the B3LYP level, the aug-cc-pVDZ and aug-cc-pVTZ basis sets yield also almost equal momentum distributions. In other words, the closely related aug-cc-pVDZ and cc-pVDZ++ basis sets must enable quantitative enough computations of momentum distributions. The employed models for the calculations of electron momentum distributions cannot be incriminated for explaining the discrepancies between theory and experiment. The interested reader is also referred further to previous works from our groups on EMS momentum distributions,[37,68] which

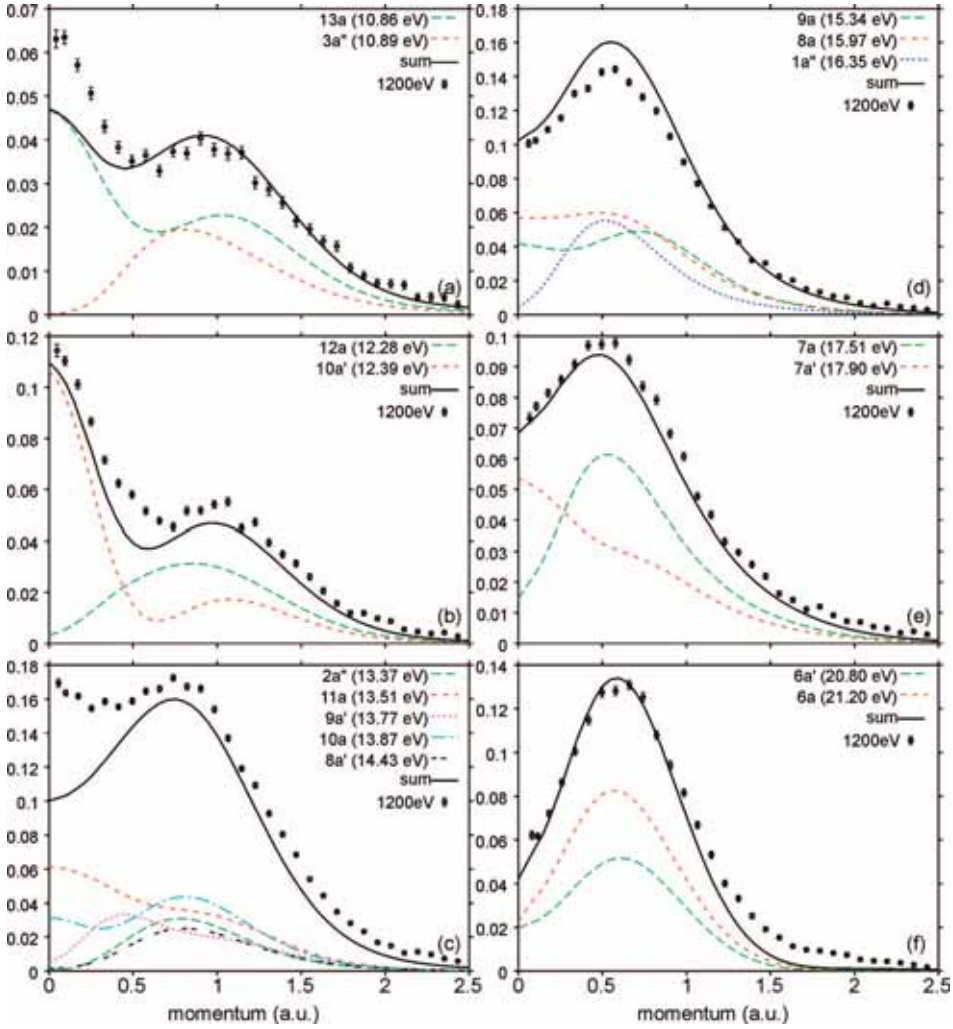

Figure 8. Decomposition of benchmark spherically and thermally averaged ADC(3)/cc-pVDZ++ electron momentum distributions ($T = 298.15$ K, $E_0 = 1.2$ keV) into individual Dyson orbital contributions: (a) band 1 ($\epsilon_b \approx 10.9$ eV), (b) band 2 ($\epsilon_b \approx 12.4$ eV), (c) band 3 ($\epsilon_b \approx 13.6$ eV), (d) band 4 ($\epsilon_b \approx 15.8$ eV), (e) band 5 ($\epsilon_b \approx 17.8$ eV), and (f) band 6 ($\epsilon_b \approx 21.0$ eV).

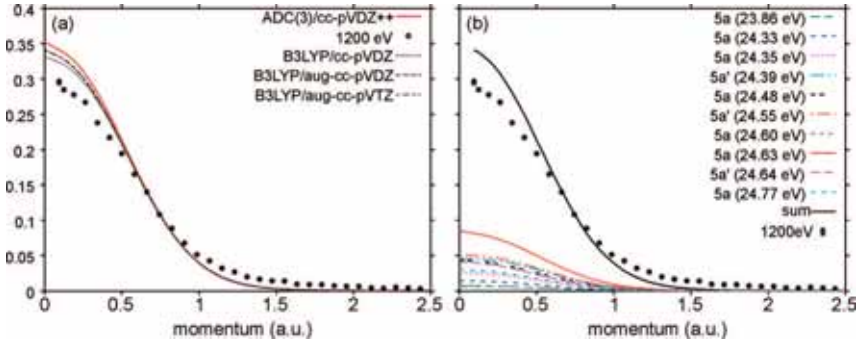

Figure 9. Analysis of the momentum distributions inferred for the C_{2s} shakeup band (band 7 at ~24.5 eV). (a) Comparison of the spherically and thermally averaged momentum profile ($T = 298.15$ K, $E_0 = 1.2$ keV) with experiment at different levels of theory. (b) Decomposition of the best ADC(3)/cc-pVDZ++ profile into individual Dyson orbital contributions.

indicate that as compared with recent and high resolution measurements, ADC(3)/cc-pVDZ++ Dyson orbital momentum distributions provide in general exceedingly accurate insights into their experimental counterparts.

In view of the resemblance of the 3a″ (HOMO) orbital of the C_s conformer with a *d* type or even a *f* type atomic orbital and in analogy with recent works on the outer-valence electron momentum distributions of ethylene,[69] difluoromethane,[37] or oxygen,[70] one may in a next step wonder whether the particularly strong discrepancies that are observed between theory and experiment for band 1 (Figures 7a and 8a) can be ascribed to distorted wave effects, that is, to a breakdown of the PWIA. Further EMS measurements at much higher electron impact energies ($E_0 = 2.4$ keV) indicate that this is not the case at all.[67] The energy gaps between the maxima characterizing bands 1−3 exceed 1.1 eV and are therefore significantly larger than the energy resolution (0.6 eV) of the employed (e, 2e) experimental set up. It seems therefore unlikely that the very significant discrepancies that are observed between the theoretical and the experimental momentum distributions characterizing

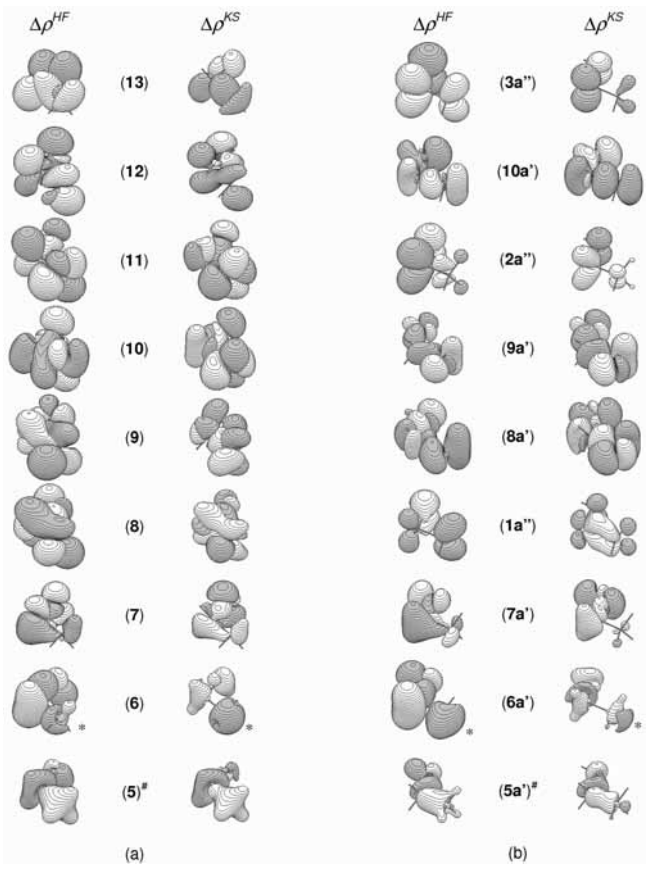

Figure 10. Contour plots of electron density differences ($\Delta\rho$) between the normalized averaged Dyson orbitals and the related RHF or RKS orbitals (see the text for an explanation). The selected values for the contours are 0.001, except *, where contours are 0.00045. The "#" superscripts emphasize a partial or complete breakdown of the orbital picture of ionization. The gray and white areas correspond to regions that exhibit an increase or decrease of the electron density, respectively. (a) C_1 conformer and (b) C_s conformer. These plots were obtained using the cc-pVDZ++ basis set and B3LYP/aug-cc-pVTZ geometries and can be readily compared with the molecular orbital contours displayed in Figure 2.

bands 1 and 3 could be explained by unusually strong overlap effects in the deconvolution of the experimental (e, 2e) ionization spectra. In view of the extremely strong influence of the molecular conformation, these discrepancies are probably indicative of a stronger structural disorder than that described in a thermodynamical model that focuses only on conformational equilibrium between the two energy minima of ethanol.

Kohn−Sham vs Dyson Orbital Densities. The observation that standard KS orbital energies yield exceedingly large underestimations of one-electron ionization energies amply justifies a systematic confrontation of Kohn−Sham orbital densities against benchmark many-body results derived from ADC(3) Dyson orbitals. A comparison with HF orbital momentum densities is also useful, as these on the contrary most commonly lead to overestimations of one-electron binding energies by a few eV, due to the neglect of electronic correlation and relaxation effects at the level of Koopmans' theorem.

Since in an exact theory of ionization, ionization cross-sections formally relate to the squared Dyson orbitals associated to the ionization states of interest, we display in Figure 10 contour plots of the electron density differences between normalized ADC(3) Dyson orbital densities and the corresponding HF (or KS) orbital densities. More specifically, these electron density differences have been computed as follows:

$$\Delta\rho^{\mathrm{HF}}(\vec{r}) = \rho^{\mathrm{ADC(3)}}(\vec{r}) - \rho^{\mathrm{RHF}}(\vec{r})$$
$$\Delta\rho^{\mathrm{KS}}(\vec{r}) = \rho^{\mathrm{ADC(3)}}(\vec{r}) - \rho^{\mathrm{RKS}}(\vec{r}) \quad (11)$$

with

$$\rho^{\mathrm{ADC(3)}}(\vec{r}) = \left[\sum_n \Gamma_n\right]^{-1} \sum_n g_n^2(\vec{r}) \quad (12)$$

where the sums on n run on all identified ionization lines that could be recovered for a given RHF molecular orbital. When the orbital picture of ionization is valid, these sums reduce to a single component only; otherwise, these sums imply an averaging of Dyson orbital densities over all of the associated shakeup satellites. In view of the MO contours displayed in Figure 2, it is rather clear that, upon comparing Dyson with HF orbitals (Figure 10), electronic relaxation in the Dyson orbitals characterizing the two outermost ionization lines yields a decrease of the electronic density in the lone-pair region. Because of the very low symmetry of the target structures, trends complicate at higher electron binding energies. Upon comparing the contour plots of the $\Delta\rho^{\mathrm{HF}}$ and $\Delta\rho^{\mathrm{KS}}$ density differences, it appears rather clearly that the ADC(3) Dyson orbitals lie in between the HF and the Kohn−Sham orbitals (note in particular the almost systematic reversal in sign of the $\Delta\rho^{\mathrm{HF}}$ and $\Delta\rho^{\mathrm{KS}}$ density plots). An obvious explanation is that, at the ADC(3) level, both electronic correlation and relaxation effects are accounted through the interplay of initial- and final-state configuration interactions, whereas only ground-state correlation is accounted for in DFT through the interplay of standard functional such as B3LYP, and both effects are neglected at the HF level (Koopmans' theorem). The trends that are observed in Figure 10 are therefore consistent with the prevailing view in the theory of ionization that for one-electron ionization states, the removal of ground-state pair correlation is approximately compensated by electronic orbital and pair relaxation effects in the final state.[29a] We note also from Figure 10 that, in spite of their deficiencies with regards to ionization energies, Kohn−Sham orbital momentum distributions are much closer to the benchmark ADC(3) results than the HF orbitals.

Conclusions and Outlook for the Future

A thorough theoretical study of the electronic structure, ionization spectrum, and electron momentum distributions of ethanol has been presented, under the assumption of conformational equilibrium in the gas phase, according to a model that focuses on a mixture of the *gauche* (C_1) and *anti* (C_s) conformers in their energy minimum forms, using weight coefficients obtained from thermostatistical calculations that account for the influence of hindered rotations. This analysis is based on exceedingly accurate calculations of the energy differences between the two conformers, at the confines of relativistic quantum mechanics, using the principles of a focal point analysis.

In a second step, the valence one-electron and shakeup ionization spectra of the two conformers have been calculated using one-particle Green's Function (1p-GF) theory in conjunction with the so-called third-order Algebraic Diagrammatic Construction scheme [ADC(3)]. A confrontation with available UPS (HeI) measurements confirms the expected accuracy of ∼0.2 eV on one-electron binding energies and the presence at electron binding energies of very significant conformational fingerprints onto outer-valence ionization energies ranging from ∼14 to ∼18 eV. The shakeup onset is located at ∼24 eV, and a shoulder at ∼14.5 eV in the He I spectrum can be specifically ascribed to the minor *anti* (C_s) conformer fraction.

In a third step, simulations at the ADC(3) level of (e, 2e) ionization spectra according to the technical characteristics of the best available set ups nowadays indicate that seven ionization bands (1−7) at electron binding energies of 10.9, 12.4, 13.6, 15.8, 17.8, 21.0, and ∼24.5 eV can be reliably resolved and analyzed in EMS experiments. These simulations indicate that at vanishingly small target electron momenta ($\tilde{\phi} = 0°$), the second band at 12.4 eV specifically relates to the minor *anti* conformer fraction, whereas bands 1, 3, and 4 at 10.9, 13.6, and 15.8 eV almost exclusively relate to the major *gauche* (C_1) conformer fraction. In a fourth and last step, thermally and spherically averaged electron momentum distributions for all resolvable bands have been correspondingly computed from Dyson orbitals obtained at the ADC(3) level and compared with preliminary EMS measurements[64] at an electron impact energy of 1.2 keV.

Whereas an increasing system size tends to enhance conformational fingerprints in ionization spectra, because of cooperative effects such as interactions between lone-pairs[1a,b,e] or anomeric interactions,[2a,b,f] π-conjugation[2d] or methylenic hyperconjugation (also referred to as σ-conjugation),[1c−f] this analysis demonstrates on the contrary that a decrease in system size is likely to exacerbate the influence of the molecular conformation on electron densities in momentum space, in particular at low electron momenta. For assessing this point, the interested reader is referred to recent studies of the electron momentum distributions of larger conformationally versatile molecules such as *n*-butane,[2c] *n*-pentane,[5] or dimethoxymethane:[2f] Never to date so large conformational fingerprints have been identified in momentum space. A similar observation can be made with regards to the influence of diffuse functions in the basis set, which have almost no discernible effect on the one-electron and shakeup ionization spectrum but which are on the contrary very much needed for accurate insights into electron densities at low momenta, thus at large distances in configuration (*r*) space. Analysis of the momentum distribution associated to band 7 at 24.5 eV confirms that this band exclusively relates to many C_{2s} shakeup satellites with individually small ionization intensities.

The influence of the molecular conformation is exceedingly strong for the momentum distributions associated to the two outermost lone-pair levels, which a comparison with experiment qualitatively corroborates. Nevertheless, the agreement between theory and experiment is somehow deceiving from a quantitative viewpoint. The most likely explanations to the observed discrepancies between theory and experiment must be sought into shortcomings of the employed model with regards to the description of thermally induced molecular motions in the neutral ground state, thus into deviations of the molecular structures away from a thermodynamical equilibrium between ground-state energy minima. According to large scale MP4 calculations, ethanol is characterized indeed by exceedingly low hydroxyl torsion barriers of 404.1 (1.15 kcal/mol) and 423.3 cm^{-1} (1.21 kcal/mol) for the *trans*−*gauche* and *gauche*−*gauche* transitions, respectively.[20] It is clear, therefore, that in a dynamical depiction many more structures associated with the hydroxyl rotations should contribute to the conformational mixture characterizing ethanol at room temperature ($k_B T = 0.58$ kcal/mol at $T = 298$ K). In view of estimated energy barriers of 1200−1300 cm^{-1} (3.4−3.7 kcal/mol), the concerted rotation of methyl groups may also play a non-negligible role. In line with a study by our group of the influence of thermally induced molecular motions on the electronic absorption spectra of large conjugated molecules,[71] we suggest in a further study to couple molecular dynamical simulations[72] with calculations of electron momentum distributions under the assumption that the one-electron picture of ionization and the target Kohn−Sham approximation are valid, a view that the present ADC(3) calculations and comparison with Kohn−Sham orbital densities or momentum distributions fully support on this occasion. A major difficulty to overcome in a dynamical averaging of ionization spectra and electron momentum distributions over several hundreds or even thousands of model molecular structures would be to be able to account for the influence of the molecular conformation on the ionization energies. Appropriate computer methodologies and exceedingly accurate classical force fields need to be developed for this purpose.

Acknowledgment. All calculations presented in this work have been performed on Compaq ES45 and ES47 work stations at Hasselt University, Belgium. This work has been supported by the FWO-Vlaanderen, the Flemish branch of the Belgian National Science Foundation, and by the BijzonderOnderzoeks-Fonds (BOF: special research fund) at Hasselt University. F.M. acknowledges the "Bijzonder OnderzoeksFond" of the Hasselt University for his Ph.D. fellowship. B.H. acknowledges financial support for his visiting postdoctoral fellowship from the FWO research community "Quantum Chemistry: Applied and Fundamental Aspects of Density Functional Theory". The work by C.G.N. and J.K.D. has been supported by the National Natural Science Foundation of China under Contracts 10575062 and 10704046 and the Specialized Research Fund for the Doctoral Program of Higher Education under Contract 20050003084.

References and Notes

(1) (a) Boulanger, P.; Riga, J.; Verbist, J. J.; Delhalle, J. *Macromolecules* **1989**, *22*, 173. (b) Hennico, G.; Delhalle, J.; Boiziau, C.; Lecayon, G. *J. Chem. Soc. Faraday Trans.* **1990**, *86*, 1025. (c) Deleuze, M.; Denis, J.-P.; Delhalle, J.; Pickup, B. T. *J. Phys. Chem.* **1993**, *97*, 5115. (d) Deleuze, M.; Delhalle, J.; Pickup, B. T.; Svensson, S. *J. Am. Chem. Soc.* **1994**, *116*, 10715. (e) Deleuze, M.; Mosley, D. H.; Delhalle, J.; André, J.-M. *Phys. Scr.* **1995**, *51*, 111. (f) Beamson, G.; Clark, D. T.; Hayes, N. W.; Law, D. S. L.; Siracusa, V.; Recca, A. *Polymer* **1996**, *37*, 379. (g) Duwez, A.-S.; Di Paolo, S.; Ghijsens, J.; Riga, J.; Deleuze, M.; Delhalle, J. *J. Phys. Chem. B* **1997**, *101*, 884. (h) Beamson, G.; Pickup, B. T.; Li, W.; Mai, S. M. *J. Phys. Chem. B* **2000**, *104*, 2656. (i) Beamson, G. *J. Electron Spectrosc. Relat. Phenom.* **2001**, *105*, 6695. (j) Beamson, G. *J. Electron Spectrosc. Relat. Phenom.* **2007**, *154*, 83. (k) Flamia, R.; Lanza, G.; Salvi, A. M.; Castle, J. E.; Tamburro, A. M. *Biomacromolecules* **2005**, *6*, 1299.

(2) (a) Neville, J. J.; Zheng, Y.; Brion, C. E. *J. Am. Chem. Soc.* **1996**, *118*, 10533. (b) Zheng, Y.; Neville, J. J.; Brion, C. E. *Science* **1995**, *270*, 5237. (c) Deleuze, M. S.; Wang, W. N.; Salam, A.; Shang, R. C. *J. Am. Chem. Soc.* **2001**, *123*, 4049. (d) Deleuze, M. S.; Knippenberg, S. *J. Chem. Phys.* **2006**, *124*, 104309. (e) Yang, T. C.; Su, G. L.; Ning, C. G.; Deng, J. K.; Wang, F.; Zhang, S. F.; Ren, X. G.; Huang, Y. R. *J. Phys. Chem. A* **2007**, *111*, 4927. (f) Huang, Y. R.; Knippenberg, S.; Hajgató, B.; François, J.-P.; Deng, J. K.; Deleuze, M. S. *J. Phys. Chem. A* **2007**, *111*, 5879.

(3) (a) Kishimoto, N.; Hagihara, Y.; Ohno, K.; Knippenberg, S.; François, J.-P.; Deleuze, M. S. *J. Phys. Chem. A* **2005**, *109*, 10535. (b) Borodin, A.; Yamazaki, M.; Kishimoto, N.; Ohno, K. *J. Phys. Chem. A* **2006**, *110*, 1783.

(4) (a) McCarthy, I. E.; Weigold, E. *Rep. Prog. Phys.* **1991**, *91*, 789. (b) Coplan, M. A.; Moore, J. H.; Doering, J.-P. *Rev. Mod. Phys.* **1994**, *66*, 985. (c) Weigold, E.; McCarthy, I. E. *Electron Momentum Spectroscopy*; Kluwer Academic Plenum Publishers: New York, 1999.

(5) Knippenberg, S.; Huang, Y. R.; Hajgató, B.; François, J.-P.; Deleuze, M. S. *J. Chem. Phys.* **2006**, *125*, 104309.

(6) (a) Cederbaum, L. S.; Domcke, W; Schirmer, J.; Von Niessen, W. *Adv. Chem. Phys.* **1986**, *65*, 115. (b) Deleuze, M. S.; Cederbaum, L. S. *Adv. Quantum Chem.* **1999**, *35*, 77. (c) Deleuze, M. S.; Trofimov, A. B.; Cederbaum, L. S. *J. Chem. Phys.* **2001**, *115*, 5859.

(7) (a) Köppel, H.; Domcke, W.; Cederbaum, L. S. *Adv. Chem. Phys.* **1984**, *57*, 59. (b) Köppel, H.; Cederbaum, L. S.; Domcke, W. *J. Chem. Phys.* **1988**, *89*, 2023. (c) Worth, G. A.; Cederbaum, L. S. *Annu. Rev. Phys. Chem.* **2004**, *55*, 127.

(8) (a) Brion, C. E.; Zheng, Y.; Rolke, J.; Neville, J. J.; McCarthy, I. E.; Wang, J. J. *J. Phys. B* **1998**, *31*, L223. (b) Takahashi, M.; Saito, T.; Hiraka, J.; Udagawa, Y. *J. Phys. B* **2003**, *36*, 2539. (c) Watanabe, N.;

Takahashi, M.; Udagawa, Y.; Kouzakov, K. A.; Popov, Y. V. *Phys. Rev. A* **2007**, *75*, 052701.

(9) Abu-Samba, M.; Børve, K. J.; Sæthre, L. J.; Thomas, T. D. *Phys. Rev. Lett.* **2005**, *95*, 103002.

(10) Cho, A. *Science* **2004**, *303*, 942.

(11) Weibel, J. D.; Jackel, C. R.; Swofford, R. L. *J. Chem. Phys.* **2002**, *117*, 4225.

(12) Coussan, C. S.; Bouteiller, Y.; Erchard, J. P. *J. Phys. Chem. A* **1998**, *102*, 5789.

(13) Fang, H. L.; Swofford, L. *Chem. Phys. Lett.* **1984**, *105*, 5.

(14) Fang, H. L.; Compton, D. A. C. *J. Phys. Chem.* **1988**, *92*, 6518.

(15) Su, C. F.; Richard Qade, C. *J. Mol. Spectrosc.* **2000**, *199*, 34.

(16) Kakar, R. K.; Quade, C. R. *J. Chem. Phys.* **1980**, *72*, 4300.

(17) Pearson, J. C.; Sarsty, K. V. L. N.; Herbst, E.; de Lucia, F. C. *J. Mol. Spectrosc.* **1996**, *175*, 146.

(18) Barnes, A. J.; Hallam, H. E. *Trans. Faraday Soc.* **1970**, *66*, 1932.

(19) Durig, J. R.; Larssen, R. A. *J. Mol. Struct.* **1989**, *238*, 195.

(20) Senent, M. L.; Smeyers, Y. G.; Domingues-Gómez, R.; Villa, M. *J. Chem. Phys.* **2000**, *112*, 5809.

(21) Ehbrecht, M.; Huisken, F. *J. Phys. Chem. A* **1997**, *101*, 7768.

(22) Coussan, S.; Bouteiller, Y.; Perchard, J. P.; Zheng, W. Q. *J. Phys. Chem. A* **1998**, *102*, 5789.

(23) Dothe, H.; Lowe, M. A.; Alper, J. S. *J. Phys. Chem.* **1989**, *93*, 6632.

(24) Görbitz, C. H. *J. Mol. Struct. (THEOCHEM)* **1992**, *262*, 209.

(25) Bakke, J. M.; Bjerkeseth, L. H. *J. Mol. Struct.* **1997**, *407*, 27.

(26) Shaw, R. A.; Weiser, H.; Dutler, R.; Rauk, A. *J. Am. Chem. Soc.* **1990**, *112*, 5401.

(27) Abu-samba, M.; Børve, K. J. *Phys. Rev. A* **2006**, *74*, 042508.

(28) Kahn, K.; Bruice, T. C. *Chem. Phys. Chem.* **2005**, *6*, 487.

(29) (a) Szabo, A.; Ostlund, N. S. *Modern Quantum Chemistry*; McGraw-Hill: New York, 1989. (b) Helgaker, T.; Jørgensen, P.; Olsen, J. *Molecular Electronic-Structure Theory*; John Wiley and Sons: Chichester, 2004.

(30) (a) Dunning, T. H., Jr *J. Chem. Phys.* **1989**, *90*, 1007. (b) Kendall, R. A.; Dunning, T. H.; Harrison, R. J. *J. Chem. Phys.* **1992**, *96*, 6796. (c) Woon, D. E.; Dunning, T. H., Jr *J. Chem. Phys.* **1994**, *100*, 2975. (d) Peterson, K. A.; Woon, D. E.; Dunning, T. H., Jr *J. Chem. Phys.* **1994**, *100*, 7410.

(31) (a) Kwasniewski, S. P.; Claes, L.; François, J.-P.; Deleuze, M. S. *J. Chem. Phys.* **2003**, *118*, 7823. (b) Deleuze, M. S.; Claes, L.; Kryachko, E. S.; François, J.-P. *J. Chem. Phys.* **2003**, *106*, 8569.

(32) (a) Douglas, M.; Kroll, N. M. *Ann. Phys* **1974**, *82*, 89. (b) Hess, B. A. *Phys. Rev. A* **1985**, *32*, 756. (c) Hess, B. A. *Phys. Rev. A* **1986**, *33*, 3742.

(33) McQuarrie, D. A. *Statistical Thermodynamics*; Harper and Row: New York, 1976.

(34) Ayala, P. Y.; Schlegel, H. B. *J. Chem. Phys.* **1998**, *108*, 2314.

(35) (a) Pickup, B. T.; Goscinski, O. *Mol. Phys.* **1973**, *26*, 1013. (b) Cederbaum, L. S.; Hohlneicher, G.; von Niessen, W. *Mol. Phys.* **1973**, *26*, 1405. (c) Cederbaum, L. S.; Domcke, W. *Adv. Chem. Phys.* **1977**, *36*, 205. (d) von Niessen, W.; Schirmer, J.; Cederbaum, L. S. *Comput. Phys. Rep.* **1984**, *1*, 57. (e) Ortiz, J. V. In *Computational Chemistry: Reviews of Current Trends*; Leszczynski, J., Ed.; World Scientific: Singapore, 1997; Vol. 2, p 1. (f) Linderberg, J.; Öhrn, Y. *Propagators in Quantum Chemistry*, 2nd ed.; Wiley-Interscience: New York, 2004.

(36) (a) Pickup, B. T. *Chem. Phys.* **1977**, *19*, 193. (b) McWeeny, R.; Pickup, B. T. *Rep. Prog. Phys.* **1980**, *43*, 1065. (c) Deleuze, M.; Pickup, B. T.; Delhalle, J. *Mol. Phys.* **1994**, *83*, 655. (d) Seabra, G. M.; Kaplan, I. G.; Zakrzewski, V. G.; Ortiz, J. V. *J. Chem. Phys.* **2004**, *121*, 4142. (e) Oana, C. M.; Krylov, A. I. *J. Chem. Phys.* **2007**, *127*, 234106.

(37) Ning, C. G.; Ren, X. G.; Deng, J. K.; Su, G. L.; Zhang, S. F.; Knippenberg, S.; Deleuze, M. S. *Chem. Phys. Lett.* **2006**, *421*, 52.

(38) Deleuze, M. S.; Cederbaum, L. S. *Int. J. Quantum Chem.* **1997**, *63*, 465.

(39) Zheng, Y.; Brion, C. E.; Brunger, M. J.; Zhao, K.; Grisogono, A. M.; Braidwood, S.; Weigold, E.; Chakravorty, S. J.; Davidson, E. R.; Sgamellotti, A.; von Niessen, W. *Chem. Phys.* **1996**, *212*, 269.

(40) Duffy, P.; Chong, D. P.; Casida, M. E.; Salahub, D. R. *Phys. Rev. A* **1994**, *50*, 4707.

(41) Parr, R. G.; Yang, W. *Density Functional Theory of Atoms and Molecules*; Oxford University Press: New York, 1989.

(42) (a) Perdew, J. P.; Parr, R. G.; Levy, M.; Balduz, J. L. *Phys. Rev. Lett.* **1982**, *49*, 1691. (b) Perdew, J. P.; Levy, M. *Phys. Rev. Lett.* **1983**, *51*, 1884. (c) Almbladh, C. O.; Pedroza, A. C. *Phys. Rev. A* **1984**, *29*, 2322. (d) Almbladh, C. O.; von Barth, U. *Phys. Rev. B* **1985**, *31*, 3231. (e) Perdew, J. P.; Levy, M. *Phys. Rev. B* **1997**, *56*, 16021. (f) Casida, M. E. *Phys. Rev. B* **1998**, *59*, 4694.

(43) (a) Chong, D. P.; Gritsenko, O. V.; Baerends, E. J. *J. Chem. Phys.* **2002**, *116*, 1760. (b) Gritsenko, O. V.; Baerends, E. J. *J. Chem. Phys.* **2002**, *117*, 9154. (c) Gritsenko, O. V.; Braïda, B.; Baerends, E. J. *J. Chem. Phys.* **2003**, *119*, 1937.

(44) (a) Becke, A. D. *J. Chem. Phys.* **1993**, *98*, 5648. (b) Lee, C.; Yang, W.; Parr, R. G. *Phys. Rev. B* **1988**, *37*, 785.

(45) (a) Casida, M. E.; Jamorski, C.; Casida, K. C.; Salahub, D. R. *J. Chem. Phys.* **1998**, *108*, 4439. (b) Tozer, D. J.; Handy, N. C. *J. Chem. Phys.* **1998**, *109*, 10180. (c) Reimers, J.; Cai, Z.-L.; Bilić, A.; Hush, N. S. *Ann. N. Y. Acad. Sci.* **2003**, *110*, 235.

(46) (a) Knippenberg, S.; Nixon, K. L.; Mackenzie-Ross, H.; Brunger, M. J.; Wang, F.; Deleuze, M. S.; François, J.-P.; Winkler, D. A. *J. Phys. Chem. A* **2005**, *109*, 9324. (b) Knippenberg, S.; Nixon, K. L.; Brunger, M. J.; Maddern, T.; Campbell, L.; Trout, N.; Wang, F.; Newell, W. R.; Deleuze, M. S.; François, J.-P.; Winkler, D. A. *J. Chem. Phys.* **2004**, *121*, 10525.

(47) Geerlings, P.; De Proft, F.; Langenaeker, W. *Chem. Rev.* **2003**, *103*, 1793.

(48) Ayers, P. W. *Theor. Chem. Acc.* **2007**, *117*, 371.

(49) Parr, R. C.; Yang, W. *J. Am. Chem. Soc.* **1984**, *106*, 4049.

(50) Fukui, K. *Science* **1982**, *218*, 747.

(51) See, for example: (a) Van Neck, D.; Waroquier, M.; Heyde, K. *Phys. Lett. B* **1993**, *314*, 255. (b) Van Neck, D.; van Daele, L.; Dowulf, Y.; Waroquier, M. *Phys. Rev. C* **1997**, *56*, 1398.

(52) (a) Martin, J. M. L.; El-Yazal, J.; François, J.-P. *Mol. Phys.* **1995**, *86*, 1437. (b) See also: Koch, W.; Holthausen, M. C. A. *A Chemist's Guide to Density Functional Theory*, 2nd ed.; V.C.H. Wiley: Weinheim, Germany, 2001. (c) Giuffreda, M. G.; Deleuze, M. S.; François, J.-P. *J. Phys. Chem. A* **1999**, *103*, 5137. (d) Giuffreda, M. G.; Deleuze, M. S.; François, J.-P. *J. Phys. Chem. A* **2002**, *106*, 8569.

(53) Kilpatrick, J. E.; Pitzer, K. S. *J. Chem. Phys.* **1949**, *17*, 1064.

(54) Mayo, S. L.; Olafson, B. D.; Goddard, W. A. *J. Phys. Chem.* **1990**, *94*, 8897.

(55) Pitzer, K. S.; Gwinn, W. D. *J. Chem. Phys.* **1942**, *10*, 428.

(56) Frisch, M. J.; GAUSSIAN03, Revision D.01; Gaussian Inc.: Pittsburgh, PA, 1998.

(57) (a) Schirmer, J.; Cederbaum, L. S.; Walter, O. *Phys. Rev. A* **1983**, *28*, 1237. (b) von Niessen, W.; Schirmer, J.; Cederbaum, L. S. *Comput. Phys. Rep.* **1984**, *1*, 57. (c) Schirmer, J.; Angonoa, G. *J. Chem. Phys.* **1989**, *91*, 1754. (d) Weikert, H.-G.; Meyer, H.-D.; Cederbaum, L. S.; Tarantelli, F. *J. Chem. Phys.* **1996**, *104*, 7122. (e) Deleuze, M. S.; Giuffreda, M. G.; François, J.-P.; Cederbaum, L. S. *J. Chem. Phys.* **1999**, *111*, 5851. (f) Deleuze, M. S. *Int. J. Quantum Chem.* **2003**, *93*, 191.

(58) Zheng, Y.; Pang, W. N.; Shang, R. C.; Chen, X. J.; Brion, C. E.; Ghanty, T. K.; Davidson, E. R. *J. Chem. Phys.* **1999**, *111*, 9526.

(59) Schmidt, M. W.; Baldridge, K. K.; Jensen, J. H.; Koseki, S.; Gordon, M. S.; Nguyen, K. A.; Windus, T. L.; Elbert, S. T. *QCPE Bull.* **1990**, *10*, 52.

(60) (a) Ruhe, A. *Math. Comput.* **1979**, *33*, 680. (b) Meyer, H.-D.; Pal, S. *J. Chem. Phys.* **1989**, *91*, 6195.

(61) (a) Liu, B. Numerical Algorithms in Chemistry, Algebraic Methods; LBL-8158, Lawrence Berkely Laboratory. (b) Tarantelli, F.; Sgamellotti, A.; Cederbaum, L. S.; Schirmer, J. *J. Chem. Phys.* **1987**, *86*, 2201.

(62) Ren, X. G.; Ning, C. G.; Deng, J. K.; Zhang, S. F.; Su, G. L.; Huang, F.; Li, G. Q. *Rev. Sci. Instrum.* **2005**, *76*, 063103.

(63) Duffy, P.; Casida, M. E.; Brion, C. E.; Chong, D. P. *Chem. Phys.* **1992**, *159*, 347.

(64) Jönsson, P.-G. *Acta Crys.* **1976**, *B32*, 232.

(65) (a) Katsumata, S.; Iwai, T.; Kimura, K. *Bull. Chem. Soc. Jpn.* **1973**, *46*, 3391. (b) Kimura, K.; Katsumata, S.; Achiba, Y.; Yamazaki, T.; Iwata, S. *Handbook of He I Photoelectron Spectra of Fundamental Organic Molecules*; Japan Scientific Society Press: 1981.

(66) Deleuze, M. S.; Cederbaum, L. S. *J. Chem. Phys.* **1996**, *105*, 7583.

(67) Ning, C. G.; Luo, Z. H.; Huang, Y. R.; Hajgató, B.; Morini, F.; Liu, K.; Zhang, S. F.; Deng, J. K.; Deleuze, M. S. *J. Phys. B: At. Mol. Opt. Phys.* **2008**, *41*, 000000.

(68) (a) Ning, C. G.; Hajgató, B.; Huang, Y. R.; Zhang, S. F.; Liu, K.; Luo, Z. H.; Knippenberg, S.; Deng, J. K.; Deleuze, M. S. *Chem. Phys.* **2008**, *19*, 343. (b) Huang, Y. R.; Hajgató, B.; Ning, C. G.; Zhang, S. F.; Liu, K.; Luo, Z. H.; Deng, J. K.; Deleuze, M. S. *J. Phys. Chem. A* **2008**, *112*, 2339. (c) Huang, Y. R.; Ning, C. G.; Deng, J. K.; Deleuze, M. S. *Phys. Chem. Chem. Phys.* **2008**, *10*, 2374.

(69) Ren, X. G.; Ning, C. G.; Deng, J. K.; Zhang, S. F.; Su, G. L.; Huang, F.; Li, G. Q. *Phys. Rev. Lett.* **2005**, *94*, 163201.

(70) Ning, C. G.; Ren, X. G.; Deng, J. K.; Su, G. L.; Zhang, S. F.; Li, G. Q. *Phys. Rev. A* **2006**, *73*, 022704.

(71) Kwasniewski, S.; François, J.-P.; Deleuze, M. S. *J. Phys. Chem. A* **2003**, *107*, 5168.

(72) Haile, J. M. *Molecular Dynamics Simulations*; John Wiley & Sons: New York, 1997.

JP804284P